RSC Advances

PAPER

View Article Online
View Journal | View Issue

Cite this: *RSC Adv.*, 2017, **7**, 1711

A novel Eu^{3+}/Eu^{2+} co-doped $MgSrLa_8(SiO_4)_6O_2$ single-phase white light phosphor for white LEDs

Xiaoli Gao, Haitao Liu,* Xinyu Yang,* Yiguang Tian,* Xue Lu and Liyuan Han

Received 25th October 2016
Accepted 29th November 2016

DOI: 10.1039/c6ra25792e

www.rsc.org/advances

A novel $MgSrLa_{8-x}(SiO_4)_6O_2$:*x*Eu (MSLSO:*x*Eu) phosphor was synthesized through a high-temperature solid-state reaction. The crystal structures, luminescent properties, fluorescence decay time, and oxygen vacancies were investigated systemically. XRD analysis shows a typical oxyapatite structure with the space group $P6_3/m$. Europium can enter crystal matrices simultaneously in the form of Eu^{3+} and Eu^{2+} and occupy nonequivalent crystallographic positions in a lattice, thus forming various optical centers. Under ultraviolet light excitation, the phosphors simultaneously show the blue-green emission of Eu^{2+} and the green-yellow-red emission of Eu^{3+}. The optimal doping content of Eu is 7.5 mol% ($x = 0.075$). White light can be realized with a CIE coordinate of (0.3664, 0.3260) by adjusting the concentration of Eu. The lifetimes of Eu^{3+} and Eu^{2+} in this study are considerably longer than those in other references. The results suggest that the MSLSO:Eu^{2+}/Eu^{3+} (0.075) phosphor is a promising candidate for white LEDs.

Introduction

White-light-emitting diodes (WLEDs) are regarded as eco-friendly light sources because of their small size, low energy consumption, high luminous efficiency, and long lifetime, and they are environmentally benign.[1,2] The most commonly used method to obtain white light is by combining a blue LED chip and a YAG:Ce^{3+} yellow-emitting phosphor.[3,4] However, this kind of WLED present numerous disadvantages, such as poor color-rendering index (CRI) and high color temperature because of the lack of a red component in the spectrum.[5] Thus, this kind of WLED cannot satisfy illumination requirements. To solve this problem, we used an ultraviolet (UV)/n-UV LED chip coated with a single-phase white-light-emitting phosphor to fabricate WLEDs.[6]

In recent years, silicate-based luminescent materials have been given considerable attention owing to their favorable luminescence properties and high chemical stability. Apatite-structure silicates are regarded as effective matrixes for the activation by rare-earth (RE) ions.[7,8] Moreover, trivalent RE (RE^{3+}) ions play an important role in producing highly efficient luminescent materials.[9–12]

Previously reported co-doped white phosphors present several shortcomings in the spectral distribution.[13–30] For the Eu^{2+}/Mn^{2+} or Ce^{3+}/Mn^{2+} co-doped systems, the intensity of the peaks are relatively weak in the green region, whereas the Ce^{3+}/Eu^{2+} or Ce^{3+}/Tb^{3+} co-doped systems are lack the red component, which will affect the overall luminescent efficiency of materials. In general, the introduction of a variety of activated ions can compensate for the lack of spectrum, whereas this method may reduce the luminous intensity and the efficiency of energy transfer among the doped ions to a certain extent. Therefore, we focus on how to improve the loss of the doping system in the spectral distribution and how to obtain white phosphors to meet the requirements of different applications.

Among the various RE element species, europium has traditionally occupied a dominant role. Luminescence of the Eu^{3+} ion originates from its $4f^6 \rightarrow 4f^6$ transition consisting of sharp lines in the red region. The positions of its emission lines are independent of the host materials. Eu^{2+} presents broad emission from the parity-allowed transitions $4f^65d^1 \rightarrow 4f^7$, which presents wide-emission range changing in the blue-green-yellow or red band. The emission band position can be tuned by selecting different host materials.[31–35] Nevertheless, only a few studies have been considered this topic, thus inspiring us to explore the luminescence properties of Eu^{2+}/Eu^{3+} co-doped single-phase white-light-emitting phosphors.

In this study, in Eu^{3+}-doped material, part of Eu^{3+} is reduced to Eu^{2+}. The crystal structures, luminescent properties, fluorescence decay time, and oxygen vacancies were investigated systemically. Finally, the phosphors simultaneously show blue emission of the Eu^{2+} ion and green-yellow-red emission of the Eu^{3+} ion under UV light excitation. Surprisingly, high energy level emission peaks of Eu^{3+} can be observed, *i.e.*, $\{^5D_1-^7F_J\ (J = 0, 1, 2)$ and $^5D_2-^7F_J\ (J = 0, 1, 2, 3)\}$, which are our biggest innovation. White light can be realized by adjusting the concentration of Eu. Results show that MSLSO:Eu^{2+}/Eu^{3+} is a promising white-emitting phosphor for WLEDs.

College of Chemistry and Materials Engineering, Wenzhou University, Wenzhou, Zhejiang, 325035, China. E-mail: lht@wzu.edu.cn; gytian@wzu.edu.cn; yangxinyu13@126.com; Tel: +86 13777780689; +86 13858851825; +86 13706654740

Experimental

Sample preparation

MSLSO doped with Eu was synthesized with a high-temperature solid phase method by calcining a mixture of La_2O_3 (99.9%), $MgCO_3 \cdot 3H_2O$ (99.99%), $SrCO_3$, Eu_2O_3 (99.99%), SiO_2 (99.9%), and H_3BO_3, where H_3BO_3 acted as flux. All calculations were performed assuming that Eu replaces La^{3+} exclusively and formally yielding MSLSO:xEu ($x = 0$, 0.05, 0.075, 0.09, 0.10, and 0.125). That is to say, $n(Mg) : n(Sr) : n(La) : n(Si) : n(Eu) = 1 : 1 : (8 - x) : 6 : x$. Subsequently, the mixture was prefired at 1000 °C for 3 h in a weak reducing atmosphere with using carbon powder. Then, the products were cooled to room temperature naturally. After grinding for second time, and the samples were calcined at 1100 °C for 4 h under the same conditions.

Characterization

The X-ray diffraction (XRD) patterns of the samples were recorded on a Bruker D8 Advance diffractometer with Cu Kα_1 radiation ($\lambda = 1.5406$ Å) in the range of $2\theta = 10$–$90°$ with the step of $\Delta 2\theta = 0.02°$ operating at 40 mA and 40 kV. The fluorescent properties of the as-obtained samples were recorded by FluoroMax-4 (HORIBA Jobin Yvon) fluorescence spectrometer with a Xe-arc lamp of 150 W power, and the lifetime was measured with a phosphorimeter attached to the main system with a Xe-flash lamp (25 W power).

Results and discussion

X-ray phase analysis

The solid solutions MSLSO:xEu ($x = 0$, 0.05, 0.075, 0.09, 0.10, and 0.125) belong to the oxyapatite structure type. According to ref. 36 the site-symmetry of atoms in $Sr_2La_8(SiO_4)_6O_2$ crystals (space group $P6_3/m$, $z = 1$) is La1-4f, Sr-4f, La2-6h, Si-6h, O-6h, O-6h, O-12i, O-2a; $z = 1$. The structure contains isolated SiO_4 tetrahedra. Oxygen O(4) in the 2a position does not enter into the composition of the tetrahedra and forms chains that are parallel to the hexagonal crystal axis.[37] On this basis, we assumed that the Mg atoms also occupy the 4f position. Europium replacing the La atoms in $Sr_2La_8(SiO_4)_6O_2$ can also be located in these two positions. In the unit cell, the six 6h sites are occupied exclusively by $6La^{3+}$, whereas the four 4f sites are randomly shared by $1Sr^{2+}$, $1Mg^{2+}$, and $2La^{3+}$.[38]

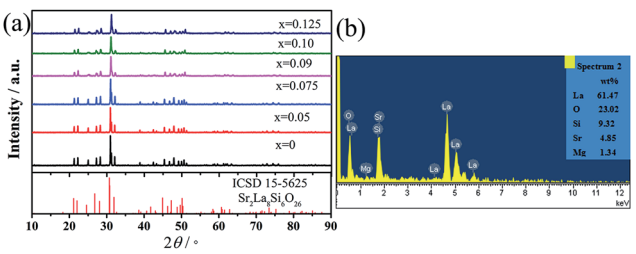

Fig. 1 (a) Powder XRD patterns of $Sr_2La_8Si_6O_{26}$ (ICSD 15-5625) and MSLSO:xEu phosphors. (b) EDS spectrum.

Fig. 1(a) shows the characteristic diffraction patterns of the synthesized solid solutions MSLSO:xEu ($x = 0$, 0.05, 0.075, 0.09, 0.10, and 0.125). All diffraction peaks of the samples can be indexed in the hexagonal unit cell, and no second phase was detected at these doping levels, indicating that all as-prepared samples matched well with that of the standard $Sr_2La_8Si_6O_{26}$ phase (ICSD card no. 155625) and all samples have hexagonal apatite-like structure with the space group of $P6_3/m$. Therefore, the doped Eu^{3+} ions present no evident influence on the crystal line structure of the host MSLSO at various Eu^{3+} doping concentrations. Fig. 1(b) shows the energy dispersive X-ray spectroscopy (EDS) spectrum of the MSLSO, which confirmed the presence of Sr, La, Mg, Si, and O elements. In addition, $n(Mg) : n(Sr) : n(La) : n(Si) : n(O) = 1 : 1 : 8 : 13 : 26$.

Photoluminescence

Fig. 2(a) illustrates that, in the PLE spectrum of 614.5 nm luminescence for the unreduced sample, two bands are centered at about 284 and 304 nm by using Gaussian fitting corresponding to the allowed $O^{2-} \rightarrow Eu^{3+}$ charge transfer state (CTS1 and CTS2) of Eu^{3+} ion. The sharp excitation peaks between 350 and 600 nm are attributed to the intra-4f transitions from the Eu^{3+} ground state $^7F_0$. Meanwhile, for the reduced samples, three bands are centered at about 267, 304, and 330 nm by using Gaussian fitting corresponding to the allowed $O^{2-} \rightarrow Eu^{3+}$ charge transfer state (CTS1 and CTS2) of Eu^{3+} ion and the $4f^7 \rightarrow 4f^65d^1$ from Eu^{2+}, respectively, as shown in Fig. 2(c). CTS1 and CTS2 correspond to the 6h sites and the 4f sites, as is consistent with the reported literature.[39] Weak sharp excitation peaks are found between 350 and 600 nm, meaning that for the emission of the Eu^{3+} ions when Eu^{2+} is excited and the CTS majorly contribute, and the contribution of f–f transition is smaller. An inflection around 290 nm of the band is centered at 330 nm, suggesting that Eu^{2+} in this site can exchange the excitation energy with Eu^{3+} probably located at the same site-type. For the reduced samples, by comparing the intensity of the peaks of the excitation spectrum, $x = 0.075$ is a more favorable condition. Next, in Fig. 2(b), we will research the emission spectra of the reduced and unreduced samples about MSLSO:0.075Eu excited at 267 and 290 nm, respectively. Compared with the unreduced sample, the reduced sample possess several sharp peaks, the intense emission peaks from transitions $^5D_1$–^7F_J ($J = 0$, 1, 2) and weak peaks from $^5D_2$–^7F_J ($J = 0$, 1, 2, 3) of Eu^{3+} appear to the emission spectra besides the peaks from $^5D_0$–^7F_J ($J = 0$, 1, 2, 3, 4) of Eu^{3+}. According to our previous experimental results, given the energy transfer from Eu^{2+} ions to the Eu^{3+} ions, high-energy level emission of Eu^{3+}. The emission spectra of the unreduced sample excited at 290 nm, where high energy level emission lines are not observed. The levels with $J = 0$ are normally not degenerated, so the $^5D_0$–$^7F_0$ transition shows no more than one band at the spectrum. Two lines for the transition $^5D_0$–$^7F_0$ indicate that the Eu^{3+} ions occupies the 4f and 6h positions.[40] According to G. Blasse,[41] for the unreduced sample, the Eu^{3+} $^5D_0$–$^7F_0$ transition is observed as the strongest peak at 577 nm and the $^5D_0$–$^7F_0$ emission of Eu^{3+} is rather intense, indicating a strong linear

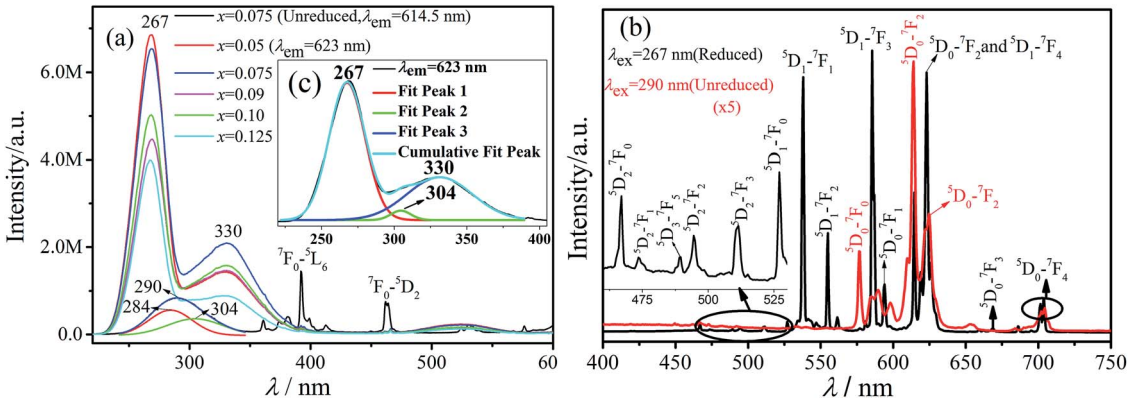

Fig. 2 (a) Excitation spectra of phosphors MSLSO:Eu^{2+}/Eu^{3+} monitored at 623 nm and MSLSO:0.075 Eu^{3+} monitored at 614.5 nm. (b) Emission spectra of the phosphors MSLSO:Eu^{2+}/Eu^{3+} (0.075) excited at 267 and 290 nm. (c) is the insert figure from (a).

Table 1 Transitions in the emission spectra of MSLSO:Eu^{2+}/Eu^{3+}

Wavelength (nm)	Transition	Wavelength (nm)	Transition
489	$^5D_3$–$^7F_5$	585.5	$^5D_1$–$^7F_3$
460	f^6d–f^7 (Eu^{2+})	623	$^5D_1$–$^7F_4$
466	$^5D_2$–$^7F_0$	577, 581	$^5D_0$–$^7F_0$
473.5	$^5D_2$–$^7F_1$	587, 589.5, 594, 598	$^5D_0$–$^7F_1$
494.5	$^5D_2$–$^7F_2$	614.5, 619, 623	$^5D_0$–$^7F_2$
511	$^5D_2$–$^7F_3$	669	$^5D_0$–$^7F_3$
527	$^5D_1$–$^7F_0$	701.5, 704	$^5D_0$–$^7F_4$
538	$^5D_1$–$^7F_1$	—	—
555, 561	$^5D_1$–$^7F_2$	—	—

crystal-field component at the Eu^{3+} ion. This case is evident in the (6h) site. The site symmetry is C_s, with one free oxygen ion in the symmetry plane. For the reduced sample, we found two bands with peaks at 577 and 581 nm (see the Table 1) for the $^5D_0$–$^7F_0$ transition, indicating that Eu^{3+} occupies two sites (6h and 4f, respectively) confirming the occurrence of two optical centers generated by Eu^{3+}. The transitions of emission spectra were identified in Table 1.[42–46]

The excitation spectra of MSLSO:Eu^{2+}/Eu^{3+} (x = 0.05, 0.075, 0.09, 0.10, and 0.125) are shown in Fig. 3(a) and 4(a) monitored at 460 nm, the excitation spectra consists of two distinct broad excitation bands peaking at 330 nm and 365 nm related to $4f^7$ ($^8S_{7/2}$) → $4f^65d^1$ from Eu^{2+}. The emission spectra of MSLSO:Eu^{2+}/Eu^{3+} (x = 0.05, 0.075, 0.09, 0.10 and 0.125) are shown in Fig. 3(b) and (c) and 4(b), in addition, the insert Fig. 3(c) is from Fig. 3(b) between 415 and 520 nm, the whole emission spectra consists of a broad emission band peaking at 460 nm related to $4f^65d^1$ → $4f^7$ ($^8S_{7/2}$) luminescence of Eu^{2+} and several sharp lines between the 530 nm and 710 nm region, ascribed to the ^5D_I → ^7F_J (I = 0, 1, 2; J = 0, 1, 2, 3, 4) transitions in Eu^{3+}. That is to say, part of the energy of Eu^{2+} transfer to Eu^{3+}, another part for its own emission; in this case, it is possible to achieve white light emission. In the oxyapatite structure,[34] Sr^{2+} occupy the 4f sites, the ionic radii of Eu^{2+} is very close to that of Sr^{2+}, moreover, the Eu^{2+} ion match the Sr^{2+} electrovalence, so it is reasonable that Eu^{2+} will substitute for Sr^{2+} to occupy the 4f sites. Thus, the energy transfer between Eu^{2+} and Eu^{3+} occurs to the 4f sites.

The above results suggest that Eu^{2+} ions play a sensitizing agent role in the emission process and also acts as an activator.

To further understand the relationship plot between the intensity of $^5D_1$, we constructed $^5D_0$ emission and the Eu^{3+} ion

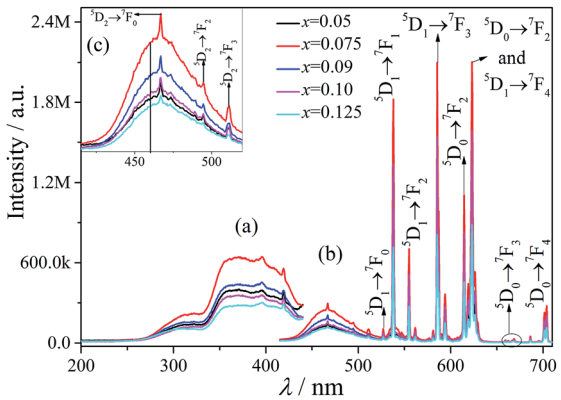

Fig. 3 (a) Excitation spectra of phosphors MSLSO:$x$$Eu^{2+}$/$Eu^{3+}$ monitored at 460 nm (monitoring the emission of Eu^{2+}). (b) The emission spectra of phosphors MSLSO:$x$$Eu^{2+}$/$Eu^{3+}$ excited at 330 nm. (c) is the insert figure from (b).

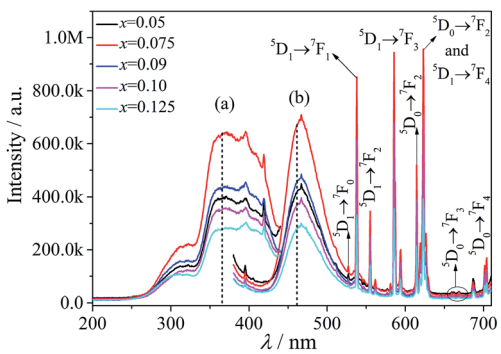

Fig. 4 (a) The range from 200 nm to 430 nm is the excitation spectra of phosphors MSLSO:$x$$Eu^{2+}$/$Eu^{3+}$ monitored at 460 nm (monitoring the emission of Eu^{2+}). (b) The range from 380 nm to 710 nm is the emission spectra of phosphors MSLSO:$x$$Eu^{2+}$/$Eu^{3+}$ excited at 365 nm.

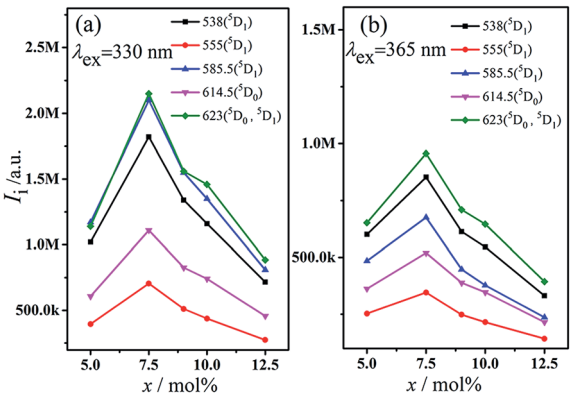

Fig. 5 Intensity of $^5D_1$, $^5D_0$ emission excited at 330 (a) and 365 nm (b) for phosphors MSLSO:xEu^{2+}/Eu^{3+} (x = 0.05, 0.075, 0.09, 0.10, and 0.125).

concentration for the luminescence intensity of $^5D_0$ and $^5D_1$ under the excitation wavelength of 330 and 365 nm, as shown in Fig. 5. Evidently, the intensity of transition ($^5D_0$ and $^5D_1$) increased with increasing Eu^{3+} ion concentration in the MSLSO host lattice from 5 mol% to 7.5 mol%; however, owing to concentration quenching, the emission intensity decreased when the Eu^{3+} ion concentration further increased over 7.5 mol%.

In summary, whether excitation spectrum or emission spectrum, the intensity of the peaks gradually increase when x = 0.075, and the intensity of the peak reached the maximum and then gradually decreases with the increasing value of x. Overall, x = 0.075 is the optimal condition.

As seen from Fig. 3(b), 4(b), and 5, the ratio of the band intensity centered at 330 nm to that of centered at 365 nm in the excitation spectrum monitored at 460 nm is close to 1/2, whereas the ratio of the intensity of several emission peaks (538, 555, 585.5, 614.5, and 623 nm) of Eu^{3+} in the emission spectrum excited at 330 nm to the same emission peaks of Eu^{3+} in the emission spectrum excited at 365 nm is close to 2. This finding shows that the energy transfer from Eu^{2+} to Eu^{3+} mainly originated from the 330 nm excitation instead of the 365 nm excitation.

Moreover, according to the emission spectrum of the MSLSO:Eu^{2+}/Eu^{3+} (0.075) excited at different wavelengths (λ_{ex} = 267, 330, and 365 nm), the chromaticity coordinate were calculated to be (0.5008, 0.4518), (0.3664, 0.3260), and (0.2300, 0.2153). The coordinates are respectively displayed in the yellow, white, and blue regions. Both spectra are fitted in the 1931CIE chromaticity diagram as shown in Fig. 6(a), indicating that the emission hue is tunable from yellow to white and eventually to blue by adjusting the excitation wavelength. Moreover, Fig. 6(b) shows the color emission spectra of sample MSLSO:Eu^{2+}/Eu^{3+} (0.075) excited at 330 nm, containing the composition of the three primary colors of white light so that white light emission is exhibited.

Fig. 7 illustrates the fluorescence decay curves of MSLSO:Eu^{2+}/Eu^{3+} (0.075) phosphor at room temperature. The experimental decay curves of MSLSO:Eu^{2+}/Eu^{3+} (0.075) can be best fitted with a double exponential eqn (1):

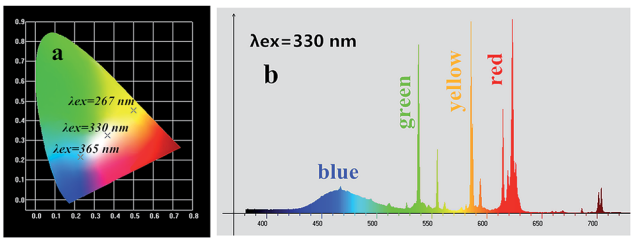

Fig. 6 (a) CIE chromaticity diagram for MSLSO:Eu^{2+}/Eu^{3+} (0.075) phosphor excited at 267, 330, and 365 nm; (b) the color emission spectra of sample MSLSO:Eu^{2+}/Eu^{3+} (0.075) excited at 330 nm.

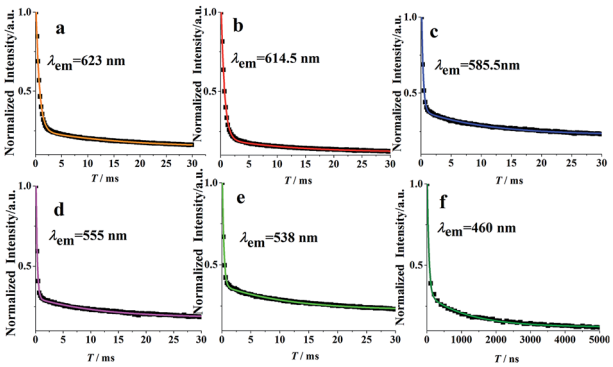

Fig. 7 Fluorescence decay curves of Eu^{2+} and Eu^{3+} emission in MSLSO:Eu^{2+}/Eu^{3+} (0.075) phosphor monitored at 623 nm (a), 614.5 nm (b), 585.5 nm (c), 555 nm (d), 538 nm (e), 460 nm (f) under excitation at 330 nm.

$$I(t) = A_1 \exp(-t/\tau_1) + A_2 \exp(-t/\tau_2) + y_0 \quad (1)$$

Suggesting the significance of the energy transfer between Eu^{3+} ions and Eu^{2+} ions, where I is the luminescence intensity, A_1 and A_2 are constants, t is the time, τ_1 and τ_2 are the decay times for the exponential components. The average decay times τ can be estimated by the following eqn (2):[47]

$$\tau = (A_1\tau_1^2 + A_2\tau_2^2)/(A_1\tau_1 + A_2\tau_2) \quad (2)$$

The fluorescence decay times of Eu^{2+} ions and Eu^{3+} ions are listed in Table 2. The lifetimes of $^5D_1$ and $^5D_0$ levels in the current study are considerably longer than those of the reports from ref. 48–51 and the lifetimes of $^5D_1$ level are longer than those of the $^5D_0$ level. We speculate that the energy transmission from $^5D_1$ to $^5D_0$ is interfered. As a result, the intense luminescence of $^5D_1$ level is achieved due to the enhanced probability of radiation transition.

Reduction of Eu^{3+} → Eu^{2+} was considered, which may be due to vacancy formation in the 4f crystal lattice position and the negative charge transfer by this vacancy to two types of Eu^{3+} ions.[39]

Fig. 8(a) displays three series of sharp peaks in the excitation spectra monitored at different wavelengths ranging from 474 nm to 655.5 nm, 382.5 nm to 523 nm, and 377.5 nm to

Table 2 Decay properties of MSLSO:Eu^{2+}/Eu^{3+} (0.075) phosphor under excitation at 330 nm

Monitored wavelength (nm)	A_1	A_2	τ_1	τ_2	τ (ms)	Fitted function
460	0.20	0.83	0.0008	0.00003	0.0007	Double exponential
538	0.92	0.15	0.18	7.96	7.01	Double exponential
555	1.09	0.12	0.15	8.10	6.95	Double exponential
586	0.89	0.16	0.19	7.51	6.60	Double exponential
614.5	0.97	0.08	0.41	8.34	5.50	Double exponential
623	0.90	0.11	0.45	11.02	8.34	Double exponential

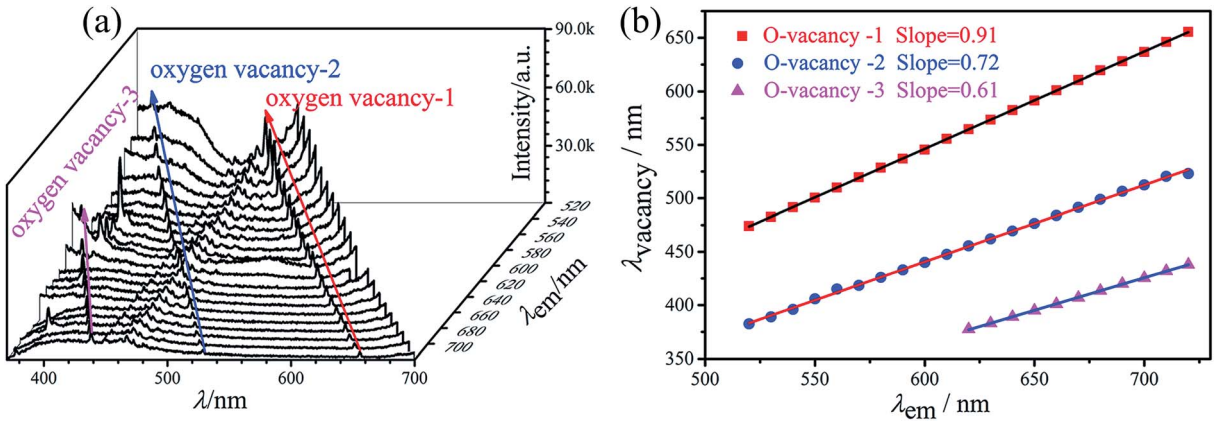

Fig. 8 (a) Excitation spectra monitored at various wavelengths and the peaks of oxygen vacancies for the MSLSO:Eu^{2+}/Eu^{3+} (0.075) are marked in arrow direction. (b) The peaks of oxygen vacancies vary from the monitor wavelengths for phosphor MSLSO:Eu^{2+}/Eu^{3+} (0.075).

438 nm, respectively. These peaks all describe a number of sharp peaks with decreasing intensity, which are brought about by absorption of radiation by oxygen vacancies. As the wavelength of detected signals increases, the luminescence maxima of the peaks are displaced to the long-wave region of the spectrum. A similar displacement of lines in the excitation spectra is described in work.[39,52,53] This displacement reflects an inhomogeneous character of oxygen vacancy distribution in the silicate matrix. Fig. 8(b) shows the peaks of oxygen vacancies vary from monitor wavelengths, the linear relationship formulas are as follows:

$$\lambda_{\text{vacancy-1}} = 0.91\lambda_{\text{moni}} + 1.10 \quad (3)$$

$$\lambda_{\text{vacancy-2}} = 0.72\lambda_{\text{moni}} + 9.76 \quad (4)$$

$$\lambda_{\text{vacancy-3}} = 0.61\lambda_{\text{moni}} - 0.99 \quad (5)$$

Under normal circumstances, transfer of energy from the $^5D_1$ level to $^5D_0$ level rapidly occurs in phosphors; therefore, the lifetime of the $^5D_1$ level is relatively short and the lines of the intense $^5D_1$ emission cannot be observed. In this host, the transfer of energy from $^5D_1$ to $^5D_0$ was hindered by oxygen vacancies; thus, the energy cannot be transmitted from $^5D_1$ to $^5D_0$. Therefore, the lines of the intense $^5D_1$ emission can be observed and $^5D_1$ level lifetimes are extremely long.

We infer two possible routes to transmit the excitation energy: one route is direct transmission to levels of Eu^{3+}, and another route is through the oxygen vacancies trapping the energy and then releasing the energy again. Direct transmission is fast, and the release process is slow. As the slow release process leading to the decay curves displayed double exponential form, we summarize these two processes as a slow process that determines $^5D_1$ level with extraordinary long lifetime and superior strength.

Conclusions

MSLSO doped with Eu phosphors were synthesized *via* high-temperature solid phase method. XRD analysis shows a typical oxyapatite structure with the space group of $P6_3/m$. The broad excitation spectra ranging from 220 nm to 430 nm, matched well with UV LED chips. Luminescence measurements indicate that the emission spectrum of as-obtained phosphors contain both the characteristic emissions of Eu^{2+} and Eu^{3+} ions, in which the broad band luminescence of Eu^{2+} and narrower 4f $\rightarrow$ 4f luminescent of Eu^{3+} can be observed upon 330 and 365 nm excitation. With increasing Eu contents, the relative intensity of the red component from Eu^{3+} become stronger gradually, whereas that of Eu^{2+} decreases, correspondingly. In addition, the optimal doping contents of Eu is confirmed to be 7.5 mol% ($x = 0.075$). Moreover, in the silicate lattice, inhomogeneously distributed oxygen vacancies are responsible for

nonradiative transfer of excitation energy. The oxygen vacancies trap and release the energy, and the release process is slow. The slow release process leads to the decay curves displayed double exponential form. The CIE chromaticity diagram for MSLSO:Eu^{2+}/Eu^{3+} (0.075) phosphor excited at 330 nm is displayed in the white region. In other words, by adjusting the concentration of Eu, the white light can be realized with the CIE coordinate (0.3664, 0.3260). Therefore, MSLSO:Eu^{2+}/Eu^{3+} (0.075) is predicted to be a promising candidate for WLEDs.

Acknowledgements

The work is financially supported by the National Natural Science Foundation of China (Grant no. 51202166).

References

1 M. Shang, X. Li and J. Lin, *Chem. Soc. Rev.*, 2014, **43**, 1372.
2 X. Bai, G. Caputo, Z. D. Hao, V. T. Freitas, J. H. Zhang, R. L. Longo, O. L. Malta, R. A. S. Ferreira and N. Pinna, *Nat. Commun.*, 2014, **5**, 5702.
3 H. J. Yu, K. Park, W. Chung, J. Kim and S. H. Kim, *Synth. Met.*, 2009, **159**, 2474.
4 C. Yang, X. J. Liang, X. X. Di, P. Z. Li, G. C. Hu, R. Cao and W. D. Xiang, *Ceram. Int.*, 2016, **42**, 14526.
5 N. C. George, K. A. Denault and R. Seshadri, *Annu. Rev. Mater. Res.*, 2013, **43**, 481.
6 K. Li, J. Fan, M. M. Shang, H. Z. Lian and J. Lin, *J. Mater. Chem. C*, 2015, **3**, 9989.
7 Y. L. Ding, Y. X. Zhang, Z. Y. Wang, W. Li, D. L. Mao, H. B. Han and C. K. Chang, *J. Lumin.*, 2009, **129**, 294.
8 C. H. Lu and P. C. Wu, *J. Alloys Compd.*, 2008, **466**, 457.
9 Y. X. Cao, G. Zhu and Y. H. Wang, *RSC Adv.*, 2015, **5**, 65710.
10 H. K. Liu, L. B. Liao, M. S. Molokeev, Q. F. Guo, Y. Y. Zhang and L. F. Mei, *RSC Adv.*, 2016, **6**, 24577.
11 D. F. Peng, Q. Ju, X. Chen, R. H. Ma, B. Chen, G. X. Bai, J. H. Hao, X. S. Qiao, X. P. Fan and F. Wang, *Chem. Mater.*, 2015, **27**, 3115.
12 D. Y. Wang, Y. J. Kang, X. C. Ye and C. B. Murray, *Chem. Mater.*, 2014, **26**, 6328.
13 C. H. Huang, T. S. Chan, W. R. Liu, D. Y. Wang, Y. C. Chiu, Y. T. Yeh and T. M. Chen, *J. Mater. Chem.*, 2012, **22**, 20210.
14 Z. Chen, J. H. Zhang, S. Chen, M. Y. Lin, C. Q. He, G. D. Xu, M. M. Wang, X. F. Yu, J. Q. Zou and K. Guo, *J. Alloys Compd.*, 2015, **632**, 756.
15 Y. Y. Zhang, Z. G. Xia, H. K. Liu, Z. Y. Wang and M. L. Li, *Chem. Phys. Lett.*, 2014, **593**, 189.
16 W. Z. Lv, M. M. Jiao, Q. Zhao, B. Q. Shao, W. Lü and H. P. You, *Inorg. Chem.*, 2014, **53**, 11007.
17 S. H. Miao, Z. G. Xia, J. Zhang and Q. L. Liu, *Inorg. Chem.*, 2014, **53**, 10386.
18 M. M. Jiao, Y. C. Jia, W. Lü, W. Z. Lv, Q. Zhao, B. Q. Shao and H. P. You, *J. Mater. Chem. C*, 2014, **2**, 90.
19 P. L. Li, Z. J. Wang, Z. P. Yang and Q. L. Guo, *J. Mater. Chem. C*, 2014, **2**, 7823.
20 N. Guo, Y. H. Zheng, Y. C. Jia, H. Qiao and H. P. You, *J. Phys. Chem. C*, 2012, **116**, 1329.
21 Y. L. Jia, R. Pang, H. F. Li, W. Z. Sun, J. P. Fu, L. H. Jiang, S. Zhang, Q. Su, C. Y. Li and R. S. Liu, *Dalton Trans.*, 2015, **44**, 11399.
22 Y. Liu, X. Zhang, Z. Hao, X. Wang and J. Zhang, *Chem. Commun.*, 2011, **47**, 10677.
23 M. M. Jiao, Y. C. Jia, W. Lü, W. Z. Lv, Q. Zhao, B. Q. Shao and H. P. You, *Dalton Trans.*, 2014, **43**, 3202.
24 W. Lü, N. Guo, Y. C. Jia, Q. Zhao, W. Z. Lv, M. M. Jiao, B. Q. Shao and H. P. You, *Inorg. Chem.*, 2013, **52**, 3007.
25 X. Y. Mi, J. C. Sun, P. Zhou, H. Y. Zhou, D. Song, K. Li, M. M. Shang and J. Lin, *J. Mater. Chem. C*, 2015, **3**, 4471.
26 M. F. Zhang, Y. J. Liang, R. Tang, D. Y. Yu, M. H. Tong, Q. Wang, Y. L. Zhu, X. Y. Wu and G. G. Li, *RSC Adv.*, 2014, **4**, 40626.
27 W. Lü, Y. C. Jia, W. Z. Lv, Q. Zhao and H. P. You, *Opt. Mater.*, 2015, **42**, 62.
28 Z. J. Wang, P. L. Li, Z. P. Yang, Q. L. Guo and G. Y. Dong, *Ceram. Int.*, 2014, **40**, 15283.
29 H. K. Liu, Y. Luo, Z. Y. Mao, L. B. Liao and Z. G. Xia, *J. Mater. Chem. C*, 2014, **2**, 1619.
30 D. L. Geng, M. M. Shang, Y. Zhang, H. Z. Lian, Z. Y. Cheng and J. Lin, *J. Mater. Chem. C*, 2013, **1**, 2345.
31 W. P. Chen, *Dalton Trans.*, 2015, **10**, 1039.
32 R. J. Yu, J. Wang, Z. Zhao, M. X. Li, S. D. Huo, J. B. Li and J. Y. Wang, *Mater. Lett.*, 2015, **160**, 294.
33 A. Baran, S. Mahlik, M. Grinberg, P. Cai, S. I. Kim and H. J. Seo, *J. Phys.: Condens. Matter*, 2014, **26**, 385401.
34 J. Sokolnicki and E. Zych, *J. Lumin.*, 2015, **158**, 65.
35 H. Bouchouicha, G. Panczer, D. deLigny, Y. Guyot, M. L. Baesso, L. H. C. Andrade, S. M. Lima and R. Ternane, *J. Lumin.*, 2016, **169**, 528.
36 Y. J. Masubuchi, M. Higuchi, T. Takeda and S. Kikkawa, *Solid State Ionics*, 2006, **177**, 263.
37 L. C. Leu, S. Thomas, M. T. Sebastian, S. Zdzieszynski, S. Misture and R. Ubicz, *J. Am. Ceram. Soc.*, 2011, **94**, 2625.
38 C. Peng, X. J. Kang, G. G. Li, Z. Y. Hou, C. X. Li and J. Lin, *J. Electrochem. Soc.*, 2011, **158**, J208.
39 M. G. Zuev, A. M. Karpov and A. S. Shkvarin, *J. Solid State Chem.*, 2011, **184**, 52.
40 M. G. Zuev, S. Y. Sokovnin, V. G. Il'ves, I. V. Baklanova and A. A. Vasin, *J. Solid State Chem.*, 2014, **218**, 164.
41 G. Blasse, *J. Solid State Chem.*, 1975, **14**, 181.
42 C. A. Kodaira, H. F. Brito, O. L. Maltab and O. A. Serrac, *J. Lumin.*, 2003, **101**, 11.
43 H. Ronde, D. M. Krol and G. Blasse, *J. Electrochem. Soc.*, 1977, **124**, 1276.
44 Y. Y. Tsai, H. R. Shih, M. T. Tsai and Y. S. Chang, *Macromol. Chem. Phys.*, 2014, **143**, 611.
45 F. Pelle, N. Gardant, M. Genotelle, P. Goldner and P. Porcher, *J. Phys. Chem. Solids*, 1995, **56**, 1003.
46 H. Yu, D. G. Deng, L. F. Chen, D. Q. Chen, J. S. Zhong, H. T. Zhao and S. Q. Xu, *Ceram. Int.*, 2015, **41**, 3800.
47 N. Ruelle, M. P. Thi and C. Fouassier, *Jpn. J. Appl. Phys.*, 1992, **31**, 2786.
48 K. H. Jang, W. K. Sung, E. S. Kim, L. Shi, J. H. Jeong and H. J. Seo, *J. Lumin.*, 2009, **129**, 1853.

49 M. D. Chambers, P. A. Rousseve and D. R. Clarke, *J. Lumin.*, 2009, **129**, 263.
50 C. Bensalem, M. Mortier, D. Vivien and M. Diaf, *Opt. Mater.*, 2011, **33**, 791.
51 M. Gaft, R. Reisfeld, G. Panczer, P. Blank and G. Boulon, *Spectrochim. Acta, Part A*, 1998, **54**, 2163.
52 G. S. Huang, X. L. Wu, Y. F. Mei, X. F. Shao and G. G. Siu, *J. Appl. Phys.*, 2003, **93**, 582.
53 F. F. Komarov, A. V. Mudryi, L. A. Vlasukova, N. I. Mukhurov and A. V. Ivanyukovich, *Opt. Spectrosc.*, 2008, **104**, 235.